Time-Resolved Small-Angle Static Light Scattering on Lysozyme during Nucleation and Growth

Patrick Umbach, Yannis Georgalis,* and Wolfram Saenger

Contribution from the Institut für Kristallographie, Freie Universität Berlin, Takustrasse 6, 14195 Berlin, Germany

Received December 18, 1996. Revised Manuscript Received September 9, 1997

Abstract: Hen egg white lysozyme was employed for studying aggregation and nucleation events induced by simple electrolytes such as NaCl while the process was monitored by time-resolved, small-angle static light scattering. The fractal dimension, the weight-average molecular weight, the mean radius of gyration and the homogeneity exponent, which typify cluster reactivity, were determined as a function of the elapse reaction time. The observed clusters resemble mass-fractals; however, direct classification to the limiting diffusion or reaction aggregation regimes is not straightforward and the findings verify deviations postulated in previous works. In nucleating solutions the interplay between packing and electrostatics makes the situation more complex than anticipated so far. A delicate balance exists between the conditions that optimize charge screening and those promoting gel formation. A nonmonotonic behavior of dimensionalities and exponents is observed when the latter are plotted as a function of lysozyme or electrolyte concentration. The implications of fractal structure formation during the nucleation of lysozyme are discussed.

Introduction

Protein crystals can be described as a solid phase dispersed in a matrix consisting of mother liquor plus excess monomeric (or oligomeric) species and other aggregate types (*i.e.*, amorphous precipitate). The route of nuclei formation is spontaneous aggregation of seeding particles allowed to diffuse and to react on collision. Under conditions that favor the diminution of repulsive interactions, some of these clusters will from critical nuclei. If the growth is allowed to follow the crystallization equilibrium path, macroscopic phase separation rather than a dispersed phase is expected to emerge. There, the formed structures are constrained by equilibrium conditions of their interfaces. The rate of the processes shifting the system back to equilibrium, is considered negligible compared to that triggering spontaneous nucleation.

Classical nucleation has been reviewed by several authors.[1−4] In brief, the free energy of monomer addition is positive for small clusters, reaches a maximum that identifies the size of the critical nucleus, and crosses to negative values for larger cluster sizes. Structures smaller than critical nuclei formed by coalescence[5,6] will be unstable and at some stage are expected to redissolve. Most of the known phenomenological approaches concern homogeneous nucleation. The conclusions are, at least partially, applicable to heterogeneous nucleation, the case most often encountered for proteins.

The examination of supersaturated protein solutions is an actual research topic (cumulative research reports can be found in congressional proceedings published in *J. Cryst. Growth* **1991**, 110; **1992**, 122 and *Acta Crystallogr*. **1994**, *D50*, 4), and it has been recently reviewed in ref 7[7]. In previous studies, we have shown that mass fractal clusters grow during nucleation of lysozyme solutions.[8−12] The appearance of the fractals is due to diminution of the repulsive potential between lysozyme molecules and the development of strong attractive interactions. Whereas the latter is a necessary step toward successful nucleation (if strong repulsive forces are present not even dimer formation is expected), there is no guarantee that equilibrium will always be driven toward crystal formation. These effects have been recently demonstrated upon induction of aggregation of lysozyme with common electrolytes frequently employed in protein crystallization such as NaCl and $(NH_4)_2SO_4$.[13,14] Since cluster growth is intimately associated with the bulk properties of the solute, in this paper we focus in more detail on the fractal clusters. The task is to identify their properties, study in detail the exponents characterizing their growth, and correlate them with the long-term fate of nucleating protein solutions.

These events can be studied by static (SLS) and dynamic (DLS) light-scattering techniques.[15−17] In conventional light-scattering equipment, the angular range of the measurements is

(1) Ohara, M.; Reid, R. C., *Modelling Crystal Growth Rates from Solution*; Prentice Hall; New Jersey; 1973.
(2) Oxtoby, D. W. *Adv. Chem. Phys.* **1988**, *70*, 263.
(3) *Fundamentals of Crystal Growth*; Hurle, D. T. J., Ed.; North Holland; Amsterdam, 1994.
(4) Ackerson, B. J.; Schätzel, K. *Phys. Rev. E* **1995**, *52* (5), 6648.
(5) Wagner, C. *Z. Elektrochem.* **1961**, *65* (7/8), 581.
(6) Landau, L. D., Lifschitz, E. M., Eds.; *Statistische Physik*; Akademie Verlag; Berlin, 1978; Vol. X, p 457.
(7) Giegé, R.; Drenth, J.; Ducruix, A.; McPherson, A.; Saenger, W. *Prog. Cryst. Growth Charact.* **1995**, *30*, 237.
(8) Georgalis, Y.; Zouni, A.; Eberstein, W.; Saenger, W. *J. Cryst. Growth* **1993**, *126*, 245.
(9) Georgalis, Y.; Saenger, W. *Adv. Colloid Interface Sci.* **1993**, *46*, 165.
(10) Georgalis, Y.; Schüler, J.; Eberstein, W.; Saenger, W. In *Fractals in the Natural and Applied Sciences*; Novak, M. M., Ed.; Elsevier Science: B. V. North-Holland, 1994; Vol. A-41, p 139.
(11) Georgalis, Y.; Schüler, J.; Frank, J.; Soumpasis, D. M.; Saenger, W. *Adv. Colloid Interface Sci.* **1995**, *58*, 57.
(12) Eberstein, W.; Georgalis, Y.; Saenger, W. *J. Cryst. Growth* **1994**, *143*, 71.
(13) Georgalis, Y.; Umbach, P.; Raptis, J.; Saenger, W. *Acta Crystallogr. D* **1997**, *D53*, 691.
(14) Georgalis, Y.; Umbach, P.; Raptis, J.; Saenger, W. *Acta Crystallogr. D* **1997**, *D53*, 703.
(15) Schmitz, S. K. *An Introduction to Dynamic Light Scattering by Macromolecules*; Academic Press: New York; 1990.

S0002-7863(96)04350-8 CCC: $15.00
Published on Web 03/03/1998

usually limited between 15° and 160°. When using DLS, this range allows for the determination of particle with the submicrometer sizes in aqueous solutions. We have reproducibly decoupled by DLS at least two populations in nucleating lysozyme solutions. The first represents lysozyme monomers (or oligomers), and the second mass fractal[18,19] clusters are more widely recognized as an amorphous precipitate. The two populations are interconnected through equilibrium conditions, and their time-resolved kinetics allow the deduction of useful screening observables. For lysozyme, it has been shown that these observables describe those solution conditions where crystallization is successful, providing crystals suitable for X-ray diffraction.[8,14]

For larger particles, measurements at smaller scattering angles are mandatory. In this work, we examined the long-time behavior of nucleating lysozyme solutions (between 1 and 6 h) using time-resolved small-angle SLS that extends the range of DLS observations. Small-angle SLS studies carry information difficult to deduce by other techniques, in terms of scaling properties of the evolving clusters. We focus on the determination of the dynamic, z, and the homogeneity, λ, exponents[20] that serve as measures of the reactivity between clusters. In previous DLS studies, z was taken to be unity at the early stages of the reaction, and thus, λ was implied to be zero (cf., eqs 6 and 7). In the present study, we find values for z larger than 1.0, and subsequently, values for λ that are larger than zero, depending on supersaturation. This indicates, at least at the later stages of the aggregation, deviations from pure diffusion-limited cluster−cluster aggregation (DLCA) despite the qualitative features of the kinetics, and we have designated the aggregation as DLCA-like.

Small-angle SLS delivers pertinent information on the aggregation kinetics, the only limiting factor being the differential settling of the clusters. If necessary, isodensity experiments can extend the observation to longer times. The implications of the deviations form the limiting regimes are discussed in the frame of lysozyme crystallization at the end of this work.

Fractal Aggregation

A substantial amount of work has been performed in the past few years in the area of colloidal aggregation, both theoretically and experimentally, especially on the relationships connecting aggregation dynamics and morphology of the resulting aggregates. Light-scattering techniques have provided pertinent information in the study of colloidal gold fractals[21−26] and the aggregation of polystyrene spheres.[27,28] Fractal clusters are observed in systems developing far from equilibrium.[29,30] Kinetic models employed for the interpretation of cluster formation do not allow for structural rearrangements. On the contrary, thermodynamic models describe growth phenomena close to equilibrium via compact structure formation. Classical phase transition models (nucleation and growth or spinodal decomposition) are based on thermodynamics, but the formation of fractal structures in kinetic growth has also been observed.[31−33]

The most widely accepted picture is that there are two limiting behaviors for both the reaction kinetics and fractal morphology of the aggregates. The parameter determining the onset of each regime is the sticking probability α between clusters. If α is equal to unity, diffusion-limited monomer−cluster (DLA) or cluster−cluster aggregation (DLCA) is expected. Values of α much smaller than unity will lead to reaction-limited monomer−cluster (RLA) or reaction-limited cluster−cluster (RLCA) aggregation. Predicted values for α are 1×10^{-9} for RLA reactions and 1×10^{-13} for RLCA.[34] Whereas the monomer−cluster model is theoretically well established, most aggregation phenomena in colloidal chemistry involve cluster−cluster reactions. It has been shown that the RLCA- and DLCA-limiting regimes exhibit universal behavior irrespective of the details on the forces responsible for the aggregation of metallic colloids, colloidal silica, and polystyrene spheres.

Solution of the Smoluchowski[18,19,35−37] equation indicates that in the DLCA regime, the growth of the average radius of gyration of the clusters obeys a power law

$$R_g(t) = R_g(0)\left[1 + \alpha \frac{t}{\tau}\right]^{z/d_f} \tag{1}$$

where z denotes a dynamic exponent, d_f is the fractal dimension and for DLCA clusters is 1.81, and α denotes the sticking probability of collision between clusters. The time constant that controls the aggregation reaction, τ, often identified as reciprocal Smoluchowski rate, is inversely proportional to the particle concentration N_0

$$\tau = \frac{3\eta}{4k_B T}\frac{1}{N_0} \tag{2}$$

where η denotes the viscosity of the solvent and $k_B T$ denotes the thermal energy. Furthermore, the growth of the weight-average mass $\bar{m}(t)$ of the clusters exhibits a linear increment with time

$$\bar{m}(t) = m_0\left(1 + 2\alpha \frac{t}{\tau}\right) \tag{3}$$

where m_0 is the mass of the seeding particle.

In contrast, for RLCA, the growth of the average radius of gyration is exponential

(16) Chu, B. *Dynamic Light Scattering*; Academic Press: New York, 1991.
(17) *Dynamic Light Scattering, the Method and some Applications*; Brown, W., Ed.; Oxford Science Publications: Oxford, 1993.
(18) van Dongen, P. G. J.; Ernst, M. H. *J. Phys. A: Math. Gen.* **1985**, *18*, 2779.
(19) van Dongen, P. G. J.; Ernst, M. H. *Phys. Rev. Lett.* **1985**, *13*, 1398.
(20) Ernst, M. H. In *Fractals in Physics*; Pietronero, L., Tosatti, E., Eds.; North Holland: Amsterdam; 1986; p 289.
(21) Lindsay, H. M.; Klein, R.; Weitz, D. A.; Lin, M. Y.; Meakin, P. *Phys. Rev. A* **1988**, *38* (5), 2614.
(22) Lindsay, H. M.; Klein, R.; Weitz, D. A.; Lin, M. Y.; Meakin, P. *Phys. Rev. A* **1989**, *39* (6), 3112.
(23) Lin, M. Y.; Lindsay, H. M.; Weitz, D. A.; Ball, R. C.; Klein, R.; Meakin, P. *Nature (London)* **1989**, *339*, 360.
(24) Lin, M. Y.; Lindsay, H. M.; Weitz, D. A.; Ball, R. C.; Klein, R.; Meakin, P. *Proc. R. Soc. London A* **1989**, *423*, 71.
(25) Lin, M. Y.; Klein, R.; Lindsay, H. M.; Weitz, D. A.; Ball, R. C.; Meakin, P. *J. Colloid Interface Sci.* **1990**, *137*, 263.
(26) Lin, M. Y.; Lindsay, H. M.; Weitz, D. A.; Klein, R.; Ball, R. C.; Meakin, P. *J. Phys.: Condens. Matter* **1990**, *2*, 3093.
(27) Carpineti, M.; Ferri, F.; Giglio, M.; Paganini, E.; Perini, U. *Phys. Rev. A* **1990**, *42* (12), 7347.
(28) Asnaghi, D.; Carpineti, M.; Giglio, M.; Sozzi, M. *Phys. Rev. A* **1992**, *45* (2), 1018.
(29) Meakin, P. In *Phase Transitions and Critical Phenomena*; Domb, C., Lebowitz, L. L. Eds.; Academic Press: New York, 1988; Vol. 12, p 351.
(30) Kolb, M. In *Large-Scale Molecular Systems*; Gans, W., Blumen, A., Aman, A., Eds.; Plenum Press: New York, 1991; Vol. 258, p 231.
(31) Carpineti, M.; Giglio, M. *Phys. Rev. Lett.* **1992**, *68* (22), 3327.
(32) Caprineti, M.; Giglio, M. *J. Phys. IV* **1993**, *3*, 39.
(33) Caprineti, M.; Giglio, M. *Phys. Rev. E* **1995**, *51* (1), 590.
(34) Vicsek, T. *Fractal Growth Phenomena*; World Scientific: Singapore, 1989.
(35) Smoluchowski, M. v. *Phys. Z.* **1916**, *17*, 557.
(36) Smoluchowski, M. v. *Phys. Z.* **1916**, *17*, 585.
(37) Smoluchowski, M. v. *Z. Phys. Chem.* **1917**, *92*, 129.

$$R_g(t) = R_g(0)\exp\left(\alpha\frac{t}{\tau}\right) \quad (4)$$

and an exponential growth of the weight-average mass of the formed clusters is expected

$$\bar{m}(t) = m_0\exp\left(2\alpha\frac{t}{\tau}\right) \quad (5)$$

RLCA clusters exhibit a fractal dimension $d_f \approx 2.1$. The fractal dimension of RLCA clusters does not enter eqs 4 and 5 and, therefore, cannot be determined from time-resolved DLS experiments as for DLCA aggregation. One can use, however, the scaling of the total scattered intensity to determine d_f (cf., eq 10).

The transition from the RLCA to DLCA regime can be typically understood as a consequence of the compression of the electric double layer surrounding the monomers.[38,39] There, cluster aggregation can occur in an intermediate fashion between RLCA and DLCA known as the cross-over regime. Scaling arguments[18,19] and experimental works[28,40] have shown that in the cross-over regime, the growth of the weight-average mass scales as a function of the dynamic exponent z

$$\bar{m}(t) \propto t^z \quad (6)$$

which in turn is associated with the homogeneity exponent λ that serves as a measure of the cluster reactivity: z and λ are interconnected with a simple relation:

$$z = \frac{1}{1-\lambda} \qquad 0 < \lambda < 1 \quad (7)$$

The value of λ is expected to be 0 for the DLCA and 1.0 for the RLCA regime. Intermediate values of λ are expected if aggregation takes place in the cross-over regime. If λ approaches unity, the system is driven toward gelation.

It should be noted that the universal DLCA and RLCA behavior is expected only under ideal conditions. For example, DLCA is the result of pure diffusion plus a sticking probability equal to unity. Interactions among clusters during the docking process would make them deviate from purely diffusive motion, and both reaction kinetics and fractal morphology will be at variance with the universality rules. In practice, most aggregating systems are likely to exhibit some degree of interaction among clusters,[41] and the predictions of universal DLCA and RLCA are considered only as the simplest limiting cases.

Light Scattering from Fractals

The SLS technique measures interference between light scattered by different points in the sample. The scattered amplitude depends on the mass of each scatterer[16] while the spatial resolution is determined by the scattering vector, q, whose magnitude is given by the Bragg condition:

$$q = \frac{4\pi n}{\lambda}\sin(\theta/2) \quad (8)$$

Here, λ (not to be confused with the symbol employed for the homogeneity exponent, cf., eq 7) denotes the wavelength of the scattered light *in vacuo*, n is the refractive index of the medium, and θ is the scattering angle. The incident and the scattered vectors define virtual fringe planes with spacing d that corresponds to the maximum dimension of the scatterer

$$d = \frac{2\pi}{q} \quad (9)$$

Particles which are aligned on these planes scatter light in the direction of the scattering angle θ.

For a given scattering vector, pairs of points separated by a distance less than π/q scatter light which is in-phase and can therefore be lumped together. The interference pattern is determined by the relative contents of small volumes of the order of π/q and separated by distances larger than π/q. If the sample is homogeneous, all of these volumes have the same mass and their contributions will cancel in the interference process. The examined solution will be transparent; otherwise, the cancellation will be incomplete and will give rise to scattering.[42,43]

Scattering techniques, when applied to fractal clusters, deliver in principle the fractal dimension, d_f, and the radius of gyration, R_g (for concentrated solutions where clusters interpenetrate each other, R_g resembles an average correlation length ξ), of the irregular fractal cluster network. At short distances, density−density correlations within single clusters are probed. The decay of the mean scattered intensity, $I(q)$, is determined in q space by the pair correlation function $g(r)$ of finding a monomer at a distance r from another monomer at the origin.[44] This probability measures the way in which a cluster fills the space; for an ensemble of randomly interconnected clusters, $g(r)$ decays as r^{D-d_f} where $D = 3$ denotes the dimension of the embedding space.[45] Consequently, the mean scattered intensity will exhibit a power−law dependence:

$$I(q) \propto q^{-d_f} \qquad \text{if } qR_g >> 1 \quad (10)$$

In comparison with neutrons and X-rays, light provides low spatial resolution because of its longer wavelength. Typically, significant phase differences are expected only when the cluster sizes are in the range between 100 nm to 1 μm. For such distances, substantial interference may occur between light rays scattered by seeding particles belonging to different fractal clusters. At these spatial scales, the largest fluctuation of segment concentration which can be observed has a size comparable to the distance between individual fractals, i.e., comparable to the radius of gyration. Hence, for scattering vectors that probe distances larger than an average correlation length, the intensity becomes independent of q. This saturation is a convenient measure of the average distance R_g between distinct fractal structures when they are studied by light scattering.

The basis for analyzing concentration fluctuations is the pair correlation function $g(r)$, defined as follows. If $c(r)$ is the concentration of seeding particles at a point, r, in the sample, the average concentration $\bar{c}$ is associated to the dimensionless volume fraction ϕ

(38) van de Ven, T. G. M. *Colloidal Hydrodynamics*; Academic Press: New York, 1989.
(39) Hunter, R. J. *Foundations of Colloid Science*; Oxford Science Press: Oxford, 1991.
(40) Olivier, B. J.; Sorensen, C. M. *Phys. Rev. A* **1990**, *41* (4), 2093.
(41) Broide, M. L. *Experimental Study of Aggregation Kinetics: Dynamic Scaling of Measured Cluster-Size Distributions*; Ph.D. Thesis, Massachusetts Institute of Technology, 1988.
(42) Kerker, M. *The Scattering of Light*; Academic Press: New York, 1969.
(43) Klems, J. K.; Freltoft, T.; Richter, D.; Sinha, S. K. *Physica* **1986**, *136B*, 285.
(44) Klein, R.; Weitz, D. A.; Lin, M. Y.; Lindsay, H. M.; Ball, R. C.; Meakin, P. *Prog. Colloid Polym. Sci.* **1990**, *81*, 161.
(45) Cabane, B. In *Neutron, X-ray and Light Scattering*; Lindner, P., Zemb, Th., Eds.; North Holland: Amsterdam, 1991; p 247.

$$\bar{c} = \phi a^{-D} \tag{11}$$

where a^D is proportional to the volume of the seeding particle. The inverse Fourier transform of $g(r)$ delivers the static structure factor $S(q)$ which is the quantity of interest in scattering experiments.[46]

$$S(q) = 1 + \bar{c}\int_0^\infty [g(r)]^{-1} \frac{\sin(q\,r)}{q\,r} 4\,\pi\,r^2\,\mathrm{d}r \tag{12}$$

Fractal structures can be described by the structure factors given by the Fisher−Burford[47] approximation:

$$S(q) = S(0)\left[1 + \frac{2(qR_g)^2}{3d_f}\right]^{-d_f/2} \quad \text{with } S(0) = \left(\frac{R_g}{a}\right)^{d_f} \tag{13}$$

For small scattering vectors, this expression is reduced to the Guinier law, from which the radius of gyration R_g and the content, $(R_g/a)^{d_f}$, of fractals can be determined

$$S(q \rightarrow 0) = S(0)\left[1 - \frac{(qR_g)^2}{3}\right] \tag{14}$$

For large scattering vectors ($qR_g >> 1$), the fractal behavior $S(q) \propto q^{-d_f}$ is recovered. Alternative schemes for static structure factors of fractal clusters have been summarized by several authors.[25,26,48,49]

The mean scattered intensity is directly proportional to the product of the static structure factor, $S(q)$, due to interparticle interactions, and the form factor, $P(q)$[15,42], which depends on the geometry of the seeding particle.

$$I(q) \propto \bar{c}P(q)\,S(q) \tag{15}$$

where $\bar{c} = N_0/V$ denotes the concentration of seeding particles in the scattering volume V for a given q. At small enough scattering angles, $P(q)$ is unity. It then holds that $I(0) \propto S(0)$, which is proportional to the weight-average molecular weight of the cluster, M_w, through the osmotic compressibility

$$S(0) = k_B T\left(\frac{\partial\bar{c}}{\partial\Pi}\right)_T \propto M_w \tag{16}$$

where Π denotes the isothermal osmotic pressure.[50]

Materials and Methods

The chemicals used in the present work were of analytical grade. NaCl p.a. grade was from Merck (Darmstadt, Germany). Hen egg white lysozyme from Sigma Chemical Co. (Deisenhofen, Germany) that was crystallized three times was dialysed against water, lyophilized, and stored at 4 °C. Purity criteria resembled those described in our previous works,[9−11] and experiments were conducted in a 0.1 M sodium acetate buffer, pH 4.25. Sample temperature was kept constant throughout (20 ± 0.01 °C) using a Lauda RC6 thermostating and a R22 Lauda feedback control units. Protein and salt were rapidly mixed in the appropriate ratio and filtered through Sartorius sterile filters, 0.2 μm pore size, into standard black glass cuvettes with 5 mm sample path length. Experiments were initiated within 1 min after the protein was mixed with the electrolyte.

Lysozyme concentration ranged from 1.03 to 5.13 mM, equivalent under nonaggregating conditions to $N_0 = 6.20 \times 10^{17}$ to 3.09×10^{18} particles per cm^{-3}. This corresponds to volume fractions ϕ between 0.024 and 0.118, assuming a radius of 2.0 nm for the monomer. Measurements were conducted at two different NaCl concentrations: 0.51 and 0.75 M. The lower electrolyte concentration resembles a concentration required for triggering aggregation, whereas the higher concentration resembles that of optimal crystallization conditions (i.e., visible crystals appear within less than 2 days above 1.55 mM lysozyme[11]).

A separate series of experiments was conducted at a constant lysozyme concentration (2.0 mM) corresponding to 1.2×10^{18} particles per cm^{-3} or to a volume fraction of 0.045. In these experiments, aggregation was induced by 0.3−0.9 M NaCl and 0.3−1.2 M $(NH_4)_2SO_4$. The reason for conducting these last two series of experiments is (i) to investigate the influence of anion type and concentration in the aggregation of lysozyme and (ii) compare the behavior of NaCl and $(NH_4)_2SO_4$, since the latter is known to promote gelation but not crystallization of lysozyme.[13,14]

Data Acquisition and Reduction

The spatial resolution of conventional static light-scattering instruments spans roughly 1 decade in q space. This range is typically between $q = 4.5 \times 10^{-3}$ and 3.5×10^{-2} nm^{-1} (assuming a wavelength of 488 nm and aqueous solutions). With our small-angle SLS apparatus,[51] light can be rapidly collected over a substantially smaller scattering vector range.

In the present configuration of the instrument, scattered light is detected by an 8-bit CCD chip (Sony ICX 039, Cheops Co., Munich). After collimation, the light passes through the sample and impinges on a 9 cm polished silicium wafer, serving as a reflecting mirror, with a hole for isolating the primary beam at zero q. The effective angular range extends from 1.09° to 10.08° corresponding to scattering vectors between 2.7×10^{-4} and 2.43×10^{-3} nm^{-1} (for aqueous solutions and the He−Ne laser wavelength, 632.8 nm). This spatial range is approximately one order of magnitude larger than that of conventional SLS and allows the study of particle sizes in the range between *ca.* 1 and 10 μm.

The scattered intensity is received by the CCD chip as a circular light spot and stored temporarily as bitmap. The acquisition time of each bitmap requires less than 200 ms: a time smaller than typical time scales of aggregation. After circular averaging, the median pixel values are stored sequentially as a function of the distance from the origin which is defined in advance using the maximum intensity of the naked laser beam for centering. The scattering vector calibration is accomplished by Fraunhofer diffraction through a pinhole of known diameter ($D = 20$ μm). The intensity minima of the diffraction pattern are defined as $\sin(\theta) = 1.22(\lambda/D)$, and the distance of each pixel from the origin is computed as a function of the scattering vector. Integration of the recorded intensities and renormalization to relative gray scale intensities are performed automatically by varying the exposure times of the CCD chip between 1×10^{-4} and 2×10^{-2} s.

Finally, the scattered intensities are compared with the attenuated intensities. The turbidity of the solution is determined with a second CCD camera placed at zero q. The corrected

(46) Ziman, J. M. *Models of Disorder*; Cambridge: London, 1979.
(47) Fisher, M. E.; Burford, R. J. *Phys. Rev. A* **1967**, *156* (2), 583.
(48) Teixeira, J. *J. Appl. Crystallogr.* **1988**, *21*, 781.
(49) Schaefer, D. W. In *Scattering, Deformation and Fracture in Polymers*; Wignall, C. D., Crist, B., Rusell, T. P., Thomas, E. L., Eds.; Materials Research Society Symposium Proceedings; Materials Research Society: Pittsburgh, PA, 1987; Vol. 79, p 47.
(50) Vrij, A.; Nieuwenhuis, E. A.; Finjaut, H. M.; Agterof, W. M. *Faraday Disc. Chem. Soc. London* **1978**, *65*, 101.
(51) Umbach, P.; Georgalis, Y.; Saenger, W. *J. Am. Chem. Soc.* **1996**, *118* (39), 9314.

scattered intensity $I_c(\theta)$ is then associated to the measured $I_m(\theta)$ intensity as described[52]

$$I_c(\theta) = I_m(\theta)\left\{\frac{\exp[\tau d/\cos\theta]\tau d[\cos^{-1}\theta - 1]}{\exp[\tau d\,(\cos^{-1}\theta - 1)] - 1}\right\} \quad (17)$$

where τ denotes the sample turbidity (it should not be confused with the time scale characterizing the aggregation, cf., eq 1). The turbidities recorded in the present work were less than 3% at the highest protein and salt concentrations employed.

The scattered light distribution $I(q)$ is plotted in a double-logarithmic manner versus the scattering vector q. Due to the massive data resulting from a single kinetic experiment (*ca*. 720 spectra), fitting to eq 13 was accomplished using automated nonlinear least-squares routines. We can extract in this way all three parameters typifying the scattered intensity distributions as a function of time: (i) the radius of gyration R_g, (ii) the zero q extrapolated intensity $I(q \rightarrow 0)$, which is in the following replaced by the more convenient expression $I(0)$, and (iii) the fractal dimension of the evolving clusters, d_f. From the time evolution of the various parameters, we can then obtain precise estimates of the exponents typifying the aggregation process using eqs 1−7.

One point must be stressed here: Small-angle SLS probes different spatial scales than conventional SLS and DLS. The time scales employed are also different due to the range of intensities detectable by our apparatus (intensities below 0.2 lx are within the background noise level). Therefore, useful images could be recorded only after roughly 20−30 min. This limit varied slightly between samples depending on supersaturation. At later stages, (*i.e*., above 6 h) the apparatus ceases to deliver useful information when the particle radii exceed some 10 μm. There are still enough points in the linear segments of the data that allow to identify the exponents unambiguously. Taken together, for nonstationary systems, small-angle SLS delivers information which is complementary but not in every respect compatible to that delivered by conventional SLS. The closer approach to zero q, however, makes small-angle SLS indispensable for discerning the growth exponents of the evolving clusters.

Results

A qualitative inspection of the raw data, plotted in semilogarithmic fashion (cf., eq 5), did not reveal the characteristic RLCA exponential form. Cross-over regions leading from RLCA to DLCA could not be clearly identified either. We have therefore employed eq 1 and transformed the raw data to double-logarithmic plots for deriving the characteristic exponents assuming DLCA-like features.

The intensity distributions were fitted with the Fisher−Burford expression. In the high-scattering vector region, all curves exhibit increasingly asymptotic behavior implying mass conservation within the scattering volume. Therefore, losses due to sedimentation can be excluded. To demonstrate the fractal behavior of lysozyme clusters, we have plotted $q\,R_g$ versus $I(q)/I(0)$ instead of $I(q)$ versus q. The latter plots allow for better assessment of the fractal dimension and indicate clearly the range span by the dimensionless quantity $q\,R_g$.[23] Two plots are depicted for intensity distributions collected with 3.5 mM lysozyme and 0.51 M NaCl, Figure 1a, and 1.4 mM lysozyme and 0.75 M NaCl, Figure 1b. A roll-off behavior is observed above $qR_g^{-1} > 3$ and extends up to $qR_g^{-1} \approx 20$.

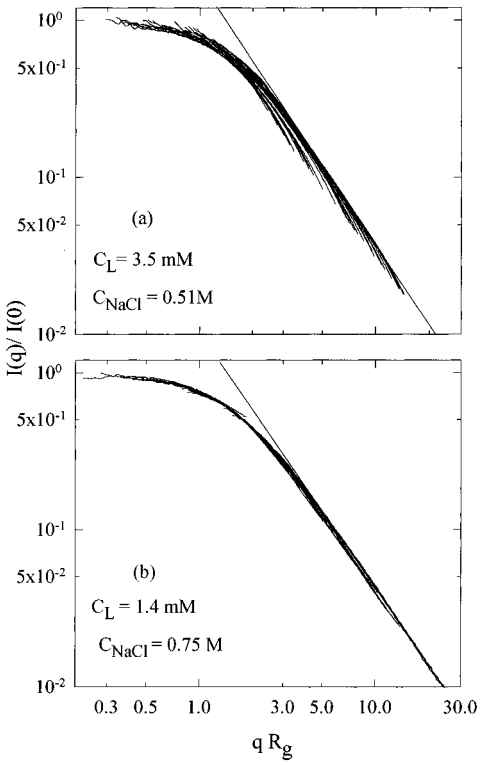

Figure 1. Typical small-angle SLS involving aggregation of the following: (a) 3.5 mM lysozyme incubated with 0.51 M NaCl and (b) 1.4 mM lysozyme incubated with 0.75 M NaCl, (b) Experiments were conducted in 0.1 M sodium acetate buffer pH 4.25 at (20 ± 0.1) °C. The first data, a, was collected for ca. 6 h and the second, b, for 14 h. For clarity, only 25 averaged images of out 720 are shown for each case. The limiting slopes, determined by linear regression to selected data segments, are −1.75 for a and −1.81 for b as indicated by the solid line. The fractal dimensions compare to those shown in Figures 7d and 8d, determined by equivalent procedures (for details see text).

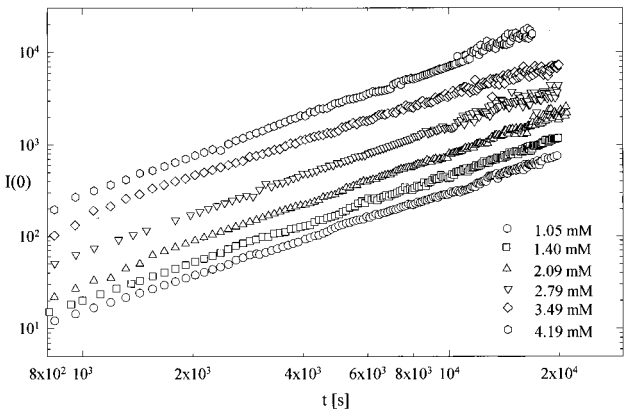

Figure 2. Time evolution of the zero-q extrapolated intensity $I(0)$; other conditions are as in Figure 1. Note that the clusters exhibit power−law growth for some 3−6 h. For clarity, only every second $I(0)$ value is plotted. The dynamic exponent, z (cf., eq 6), depicted in Figure 7a was obtained by linear regression.

The time evolution of $I(0)$ corresponding to the 0.51 M NaCl samples, is shown in Figure 2. All data sets indicate a linear behavior which extends more than 1 order of magnitude in time, from 10^3 to 20^4 s, for the indicated lysozyme concentration range. The data were fitted by a power−law dependence to determine the dynamic exponent z (cf., eq 6). We found z to

(52) Hashimoto, T.; Itakura, M.; Hasegawa, H. *J. Chem. Phys.* **1986**, *85*, 6118.

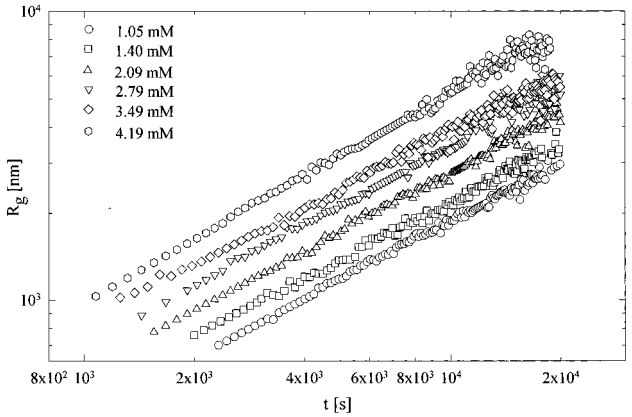

Figure 3. Time course of the mean radius of gyration R_g of lysozyme clusters; other conditions are as in Figure 1. For clarity, only every second R_g value is plotted. Note that the clusters exhibit power−law growth, the ratio z/d_f (cf., eq 1), depicted in Figure 7c, was obtained by linear regression.

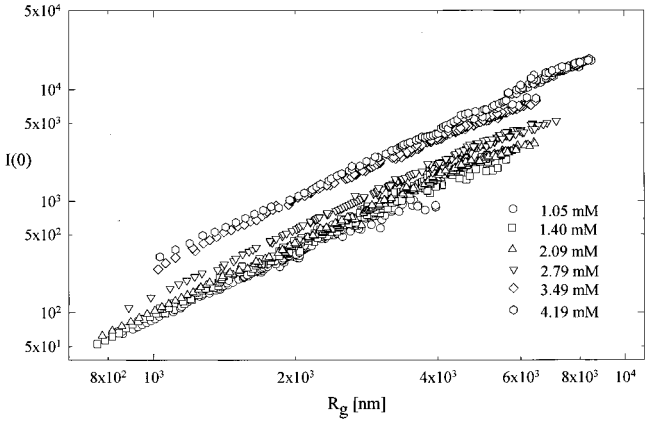

Figure 4. Plot of the zero q extrapolated intensity $I(0)$ versus radius of gyration, R_g, of the lysozyme clusters for the 0.51 M NaCl data set. For clarity, only every second $I(0)$ and R_g pair is plotted. The mean cluster fractal dimension, d_f, obtained (cf., eq 17) is 1.97 ± 0.05.

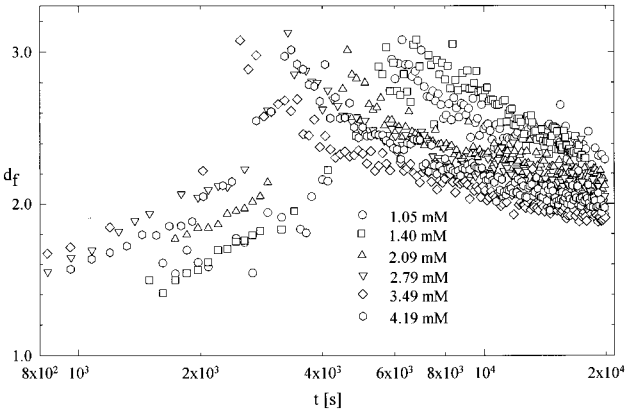

Figure 5. Evolution of the fractal dimension determined from Fisher−Burford fit to the intensity distributions for the 0.51 M NaCl series of experiments; other conditions are as in Figure 1. Note that the fractal dimension increases within the first hour to values close to 3.0, indicative of compact structures, and then relaxes between 2.00 and 2.20, depending on supersaturation.

vary between 1.3 and 2.0 for the 0.51 M NaCl data set and between 1.4 and 1.8 for the 0.75 M NaCl data set.

According to eq 7, for the 0.51 M NaCl series we obtain values of z and λ that deviate significantly from 1 and 0, respectively (*i.e.*, z ranges between 1.25 and 2.0 and λ between 0.22 and 0.50). We cannot attribute DLCA characteristics to this aggregation type. Similar behavior is exhibited by the experiments carried out in 0.75 M NaCl. There, the values of z were found to range between 1.5 and 2.12 and that of λ between 0.33 and 0.52.

The time evolution of R_g for the 0.51 M NaCl series is displayed in Figure 3. The records indicate a linear behavior which extends more than 1 order of magnitude in time, from 10^3 to 20^4 s, for the indicated lysozyme concentration range. In the linear segment, the mean cluster radii grow with a characteristic exponent z/d_f (cf., eq 1). We found z/d_f to vary between 0.65 and 0.76 for 0.51 M NaCl and between 0.85 and 1.05 for 0.75 M NaCl.

Although R_g values cannot be extrapolated to small enough times, as in DLS experiments, the intercepts of the linear parts of the curves in Figure 3, indicate $R_g(t \rightarrow 0)$ values varying between 4.3 and 5.2 nm for the 0.51, and between 3.6 to 6.5 nm for the 0.75 M NaCl series of experiments. These values provide a tentative estimate of the radius of gyration of the seeding particles. The hydrodynamic radii R_h of the seeding particles may vary between 4.7 and 8.4 nm, assuming spherical shape. The values for R_h obtained from DLS experiments are two to three times higher; it should, however, be kept in mind (i) that DLS measurements, at a single scattering angle, carry only minimal information and (ii) that quite different particle distributions are captured by each technique as function of time.

An independent measure of the fractal dimension can also be obtained for the interrelation of the zero q extrapolated scattered intensity $I(0)$ and the mean cluster radius of gyration R_g through

$$I(0) \propto R_g^{d_f} \tag{18}$$

The latter expression was further used for determining independently estimates of the fractal dimension from the linear segments of the combined data, as shown in Figure 4. The values obtained from this extrapolation indicated again a mean fractal dimension around 2.0 ± 0.1 for 0.51 M and $d_f = 1.85$ ± 0.1 for 0.75 M NaCl in fair accordance with those directly determined from the Fisher−Burford fits. Another independent determinations of the fractal dimension can be derived from the high q (asymptotic) regions of the intensity distributions. Linear least-squares fits in these regions suffice for providing d_f estimates in acceptable agreement to those determined from the Fisher−Burford fits.

The time evolution of d_f, determined from the Fisher−Burford fits to the data, is displayed in Figure 5. Obviously, the morphology of the clusters obeys a complex time behavior. The fractal dimension starts from values above 1.5 crosses to 3.0 (compact structures) and drops again to 2.0 (fractals). A pronounced maximum occurs between 2×10^4 and 6×10^4 s depending on the starting lysozyme concentration. Considerable restructuring takes therefore place in the beginning of each experiment. Systematic deviations emerging from the fitting procedure were carefully examined in these regions to exclude artefacts. Similar behavior was exhibited by the 0.75 M NaCl data set; there, the mean fractal dimension was 1.81 ± 0.02. These results are discussed in more detail following decoupling the contribution of z and d_f (see Discussion and Figures 7d−10d).

Upon completion of the light scattering experiments, the cells were examined under a high-resolution optical microscope (Axiovert-100 Zeiss, Germany) as previously described.[51] At lysozyme concentrations below 1.55 mM, only fractals could be observed for the next 2 days after the light-scattering

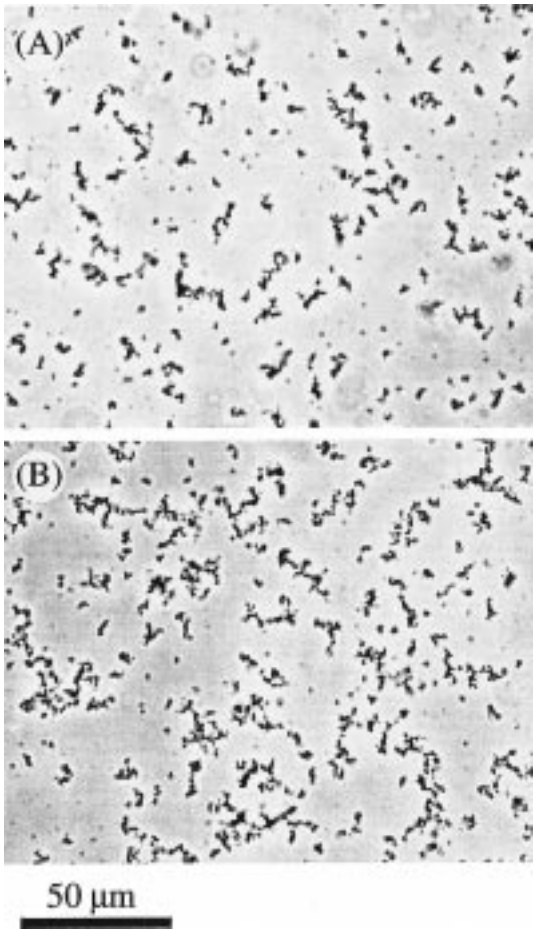

Figure 6. Typical fractal clusters grown using 3.5 mM lysozyme and (a) 0.75 M NaCl or (b) 1.1 M $(NH_4)_2SO_4$. Images were recorded after 6.0 and 23 h, respectively; other conditions are as in Figure 1.

experiments, Figure 6. For higher lysozyme concentrations, fractals coexisted with crystals. Gelation was not obvious in any of the solutions within the examined times. The displayed pictures should be considered only qualitatively and cannot be directly correlated to the small-angle SLS experiment.

Correlation of the Exponents with the Nucleation of Lysozyme

We summarize below the behavior of the dynamic exponent z, of the ratio z/d_f, of the homogeneity exponent λ, and of the decoupled net d_f for lysozyme clusters in the concentration range between 1.03 and 5.13 mM. In Figure 7 we display the 0.51 M NaCl and in Figure 8 the 0.75 M NaCl series of experiments. In Figures 9 and 10, we display the series of experiments at constant 2.0 mM lysozyme, studied as a function of (i) NaCl concentrations in the range between 0.30 and 0.90 M and (ii) $(NH_4)_2SO_4$ in the range between 0.3 and 1.1 M.

The exponents indicate a nonmonotonic behavior when plotted as a function of lysozyme or NaCl concentration, and the values derived for both z and λ deviate from the theoretically expected values for pure DLCA. For the 0.51 M NaCl data set, both z and λ exhibit a maximum at 2.0 mM lysozyme and then asymptotically escape to values typical for gelation kernels, Figure 7a,b. The 0.75 M NaCl series, Figure 8a,b, indicates a similar behavior. A maximum for both z and λ appears again at 2.0 mM lysozyme. Similar considerations apply when the exponents are plotted as a function of NaCl or $(NH_4)_2SO_4$ molarity, Figures 9a,b and 10a,b; z and λ reach a minimum value between 0.50 and 0.70 M for each salt, respectively.

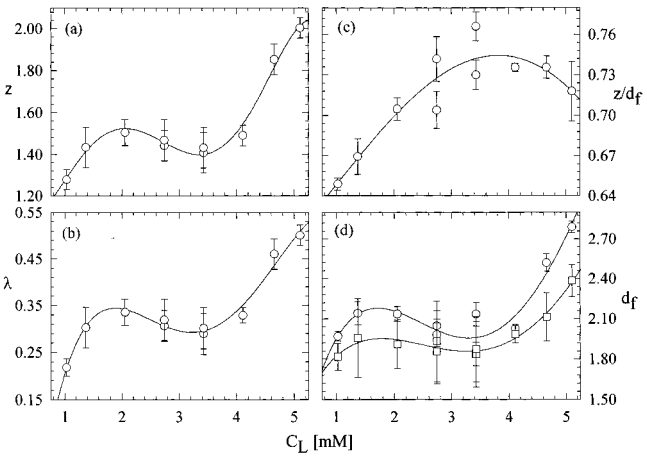

Figure 7. Exponents typifying the aggregation of lysozyme in the range between 1.03 and 5.13 mM induced by 0.51 M NaCl; other conditions are as in Figure 1. (a) Dynamic exponent z determined from the time evolution of the zero-time extrapolated scattered intensity (cf., eq 6). (b) Homogeneity exponent λ determined from the data in a (cf., eq 7). (c) Ratio z/d_f determined from the time evolution of the mean cluster radius of gyration (cf., eq 1). (d) (○) Net fractal dimension determined from the combination of data in panels a and c. (□) Fractal dimension determined from the scaling of zero q extrapolated intensity, $I(0,t)$ on the mean cluster radius of gyration R_g (cf., eq 17). The lines through the data points serve only as guides to the eye.

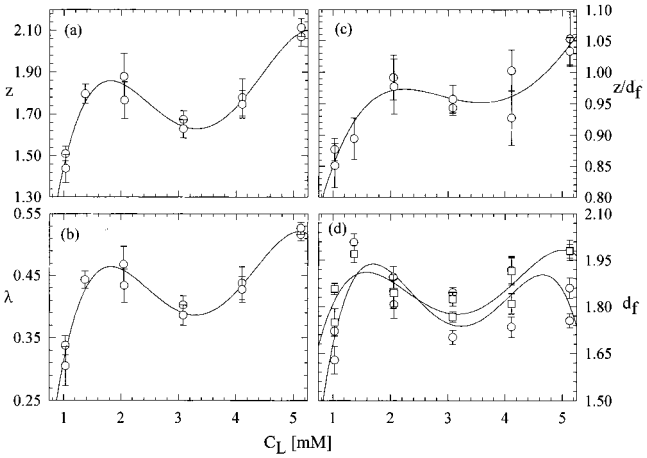

Figure 8. Exponents typifying the aggregation of lysozyme in the range between 1.03 and 5.13 mM induced by 0.75 M NaCl. Legends are identical to those of Figures 7a−d.

An inspection of the graphs indicates that cluster reactivity increases, either at the limit of high lysozyme or high salt concentration. This behavior can be understood as a tendency of crossing over to values of λ that typify the gelation transition. Values of λ equal to unity will be attained at very high lysozyme molarities such as 8 mM for the 0.51 M and 12 mM for the 0.75 M NaCl series. Similarly, for the experiment involving variation of NaCl concentration, λ will be unity between 1.70 and 2.0 M salt. These estimates are only approximate and have been deduced from Figures 7b and 8b, by linear regression at the last few data points. Interestingly, when aggregation is induced by 0.51 or 0.75 M NaCl, the protein concentrations at which λ approaches unity indicate a tendency opposite than expected since gelation should be promoted by increasing the lysozyme concentration. Some plausible explanations for this behavior may involve interactions between fractals and cluster polarization effects[41,53,54] or restructuring (see also the discussion

(53) Jullien, R. *Phys. Rev. Lett.* **1985**, *55*, 1697.

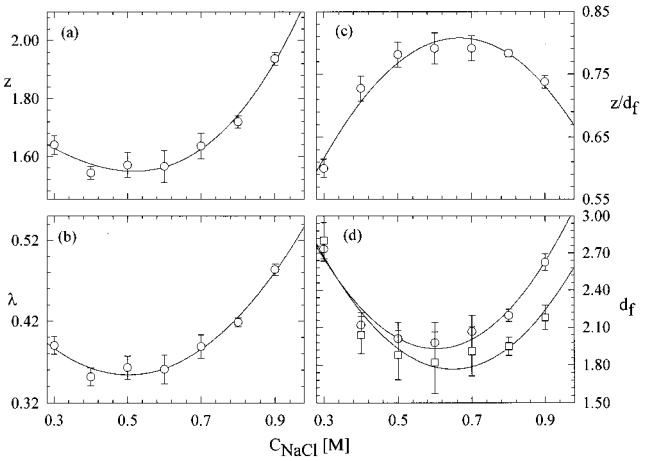

Figure 9. Exponents typifying the aggregation of 2.0 mM lysozyme at induced by NaCl ranging from 0.30 to 0.90 M. Legends are identical to those of Figures 7a−d.

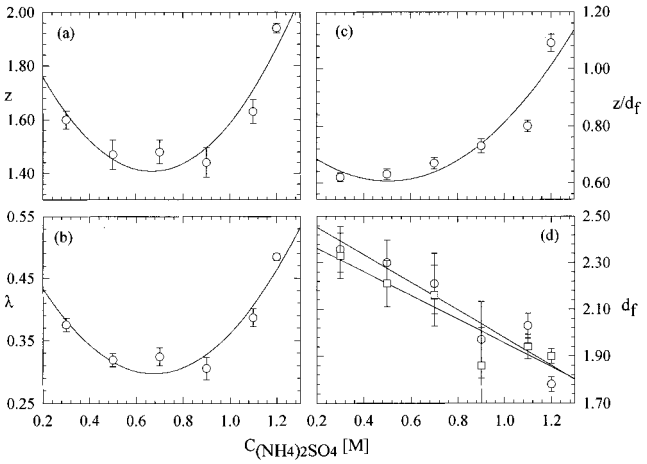

Figure 10. Exponents typifying the aggregation of 2.0 mM lysozyme induced by $(NH_4)_2SO_4$ ranging from 0.30 to 1.1 M. Legends are identical to those of Figures 7a−d.

of Figures 9 and 10). We have tried to extend the data collection in these regimes but with limited success. There, the experiments are prohibited due to showers of microcrystals and a very rapid approach to the criticality. An account on these results will be given in a separate publication.[55]

The behavior of z and λ, as depicted in Figures 9 and 10, cannot be explained in a straightforward manner. When plotted as a function of salt molarity, λ reaches a minimum at around 0.50 M NaCl. Above this molarity, λ increases again. The salt concentration at the minimum coincides with the salt molarity for igniting aggregation of lysozyme.[12] The salient feature is that the cluster reactivity increases again by increasing the salt molarity. For low volume fractions of aggregating latex particles, an opposite tendency has been shown.[28] There, the transition from RLCA to DLCA was facilitated by increasing the salt concentration and improving the effective charge screening.

The unusual behavior observed in Figures 9 and 10 may have its origin in the following sources: an increment of electrolyte concentration renders collisions between clusters more effective, through better charge screening, and the exponents show a tendency to cross to those typifying gelation, above 0.60 M NaCl. This electrolyte concentration seems to be necessary for optimizing nucleation through compression of the Debye−Hückel layer and improve screening of the repulsive interactions. However, screening depends on both concentration and nature of the electrolyte and exhibits a complex dependence in the potential of mean force that cannot be predicted by classical DLVO[56] theory due to solvent mediated interactions. Increment of salt concentration (i.e., of NaCl) does not improve screening in a monotonic fashion but gives rise to repulsive barriers above 0.5 M NaCl as shown in a recent computational study.[57]

After combining the values of z (cf., eq 6) with the values of z/d_f (cf., eq 1) and the fractal dimensions obtained directly from the scaling of $I(0,t)$ on R_g (cf., eq 18), we obtain net fractal dimensions for lysozyme concentrations in the range of 1.55−4.13 mM, between 1.97 ± 0.17 and 2.05 ± 0.12 for the 0.51 M NaCl series which corroborate closely the prevalence of RLCA kinetics, Figure 7d. In contrast, the fractal dimensions of the 0.75 M NaCl series ranges between 1.81 ± 0.11 and 1.83 ± 0.06 for the same lysozyme concentrations and resembles DLCA kinetics, Figure 8d. The fractal dimensions for the NaCl variation again indicate RLCA kinetics. The fractal dimension in these experiments ranged between 2.08 ± 0.14 and 2.24 ± 0.15 at NaCl concentrations between 0.50 and 0.80 M.

The values for d_f, usually attributed to RLCA aggregation, are in contrast with the time evolution of the radii of gyration which qualitatively exhibit DLCA power−law kinetics. Asnaghi et al.[28] have interpreted similar effects observed in polystyrene latex aggregation with a faster response of the fractal cluster morphology to sticking probability than to kinetics per se. The change of the fractal dimension, during the reaction, is also in contrast with the definition of fractal structures as invariant self-similar objects. However, if we consider small clusters evolving in time, both the number of contacts and the collision probability will increase with time. Such clusters will then fail to interpenetrate each other as if they were small. Therefore, the growth of more tenuous structures with lower fractal dimensions, as time proceeds, is not unexpected due to the increased number of collisions at the periphery of the large clusters.

These considerations indicate that the interplay between packing and electrostatics makes the situation more complex than anticipated when solvent mediated interactions are neglected. Figures 7−10 indicate that a delicate balance exists between conditions that optimize charge screening and conditions that facilitate gel formation or other transitions. The values of z or λ at the extrema may well correspond to optimal crystallization conditions for lysozyme if they indeed signify cross-overs between the optimal charge screening and the onset of the gelation transition. Based on these considerations, one can confine the range of protein and electrolyte concentrations around 2.0 mM lysozyme and 0.60 M NaCl. These estimates are following those determined in our previous studies where the same variable space was explored by time-resolved DLS.[11] Within practically the same range, we reproducibly obtain large well-diffracting lysozyme crystals with tetragonal space group. Whereas these results may not yet capture completely all nucleation events, we believe that the deduced information is useful, reasonably precise, and, most importantly, difficult to attain with other techniques.

(54) Jullien, R. J. *Phys. A* **1986**, *19*, 2129.
(55) Georgalis, Y.; Umbach, P.; Soumpasis, D. M.; Saenger, W. Submitted for publication.
(56) Verwey, E. J. W.; Overbeek, J. Th. G. *Theory of the Stability of Lyophobic Colloids*; Elsevier: Amsterdam, 1948.
(57) Soumpasis, D. M.; Georgalis, Y. *Biophys. J.* **1997**, *72*, 2770.

Discussion

Techniques such as small-angle SLS can be employed for probing later stages of lysozyme aggregation and concomitant nucleation. For a consistent picture associating nucleation and fractal cluster formation, one can imagine a scenario starting with the nucleation burst when protein and salt solutions are mixed. Nucleus−nucleus collisions then trigger catastrophic random aggregation that dominates the light-scattering process in its early stages. We have previously shown that the clusters detected by DLS, SLS, and scanning force microscopy are composed of seeding particles much larger than the lysozyme monomer.[13,14,58,59] Only a minority of the formed nuclei escapes the "Smoluchowski sink" to promote crystal formation.

The question whether the nuclei formed at the early stages are compact or ramified is not easy to answer. Most probably, the real critical size lies below the extrapolated $R_g(0)$ values, and pure nucleation that may take place in the millisecond range (depending on supersaturation), is practically inaccessible to both DLS and SLS. Yet, there is no much experimental evidence showing that nuclei are indeed compact. Theoretical studies[60−62] have indicated that deviations from the classical picture are not improbable. The fractal morphology of the clusters developing in nucleating protein solutions poses the question whether formation of fractal structures is an unavoidable step toward nucleation. If interactions between monomers are nonspecific, the case most often encountered in protein crystallization, long times will be required for proper alignment of the molecules to ordered structures. Therefore, random aggregation (fractal or amorphous precipitate formation) will be energetically favored more than nucleation via coalescence. Nuclei may then form via aimed restructuring of the fractal clusters. This postulate is supported only by few experimental studies.[63] The picture emerging from our conventional studies SLS,[12,13] and the experimental results described in the present study are very similar to the observations made by Dokter et al.[64] on zeolites where growth of nuclei and restructuring of fractals alternate. For lysozyme under crystallization conditions, this issue is, however, still under investigation.[51,58]

An obvious point emerging from the present and other studies is that detailed knowledge of the nucleation and aggregation events over wide spatiotemporal scales is necessary. The present work should be understood only as an attempt toward a better comprehension of the events taking place during biomolecular crystallization. We believe that small-angle SLS measurements on nucleating solutions will have a strong impact on the issue of protein crystallization. Most important, the extrema for the exponents appear again at those solution conditions where crystallization of lysozyme is optimal. However, an exact interpretation of these effects, which is embedded in the frame of effective many body interactions, should await further theoretical progresses.

Acknowledgment. The financial support to Y.G. from the Deutsche Forschungsgemeinschaft (Sa 196/26-1) and to P.U. from the DESY 05 641KEB project is acknowledged. We also thank M. Giglio and his group for inspiring these studies.

JA964350Q

(58) Schaper, A.; Georgalis, Y.; Umbach, P.; Raptis, J.; Saenger, W. *J. Chem. Phys.* **1997**, *106* (20), 8587.
(59) Niimura, N.; Minezaki, Y.; Ataka, M.; Katsura, T. *J. Cryst. Growth* **1995**, *154*, 136.
(60) Heermann, D. W.; Klein, W. *Phys. Rev. Lett.* **1982**, *50* (14), 1062.
(61) Klein, W.; Leyvraz, F. *Phys. Rev. Lett.* **1986**, *57* (22), 2845.
(62) Yang, J.; Gould, H.; Mountain, R. D. *J. Chem. Phys.* **1990**, *93* (1), 711.
(63) Brune, H.; Romainczyk, C.; Röder, H.; Kern, K. *Nature* **1994**, *369*, 469.
(64) Dokter, W. H.; van Garderen, H. F.; Beelen, T. P. M.; van Santen, R. A.; Bras, W. *Angew. Chem.* **1995**, *107* (1), 122.